Propulsion by Absorption of Laser Radiation

A. N. PIRRI,* M. J. MONSLER,† AND P. E. NEBOLSINE‡
Avco Everett Research Laboratory, Inc., Everett, Mass.

The results of an experimental study of the physics of propulsion by absorption of radiation from a remotely stationed high-power laser are presented. Both pulsed and steady-state simulation experiments were performed utilizing a megawatt peak power pulsed CO_2 laser. The steady-state simulation experiments were carried out in a vacuum chamber with graphite, Lucite and lithium fluoride as solid propellants. The pulsed experiments consisted of ballistic pendulum measurements of thrust, wall pressure traces, and streak camera records of plasma velocity to deduce the efficiency of a laser powered pulsejet, where air is utilized as fuel. Results indicate that for steady-state propulsion a high ratio of thrust to laser power (~10–100 dynes/w) can be obtained by using the laser to simply vaporize a suitable solid propellant. However, for high specific impulse (~1000 sec) it is necessary to add energy to the vapor in a stable manner. This may require gaseous propellants with external control over the absorption characteristics for stable heating in a throatless nozzle. The pulsejet experiments resulted in a ratio of thrust to laser power ~25 dynes/w. In order to increase the efficiency of propellant mass utilization, shorter laser pulses with higher power are desirable.

Nomenclature

A = area
C = coupling coefficient
E = laser energy
g = acceleration of gravity
I = impulse
I_{sp} = specific impulse
K = absorption coefficient
$\dot{m}$ = propellant mass flow rate
M = mass loss of propellant
P = laser power
p = pressure
R = radius of plasma
T = thrust
t = time
u = particle velocity
ρ = density
η = power conversion efficiency
τ_p = pulse time
τ_e = mass expulsion time

Subscripts

1 = in front of shock
2 = behind shock
e = exit plane
a = air

I. Introduction

THE concept of propelling a vehicle by absorbing radiation from a remotely stationed high-power laser was introduced by Kantrowitz.[1,2] While admittedly speculative at this time, the utility of this concept deserves careful evaluation, particularly for launching high volume, small payloads into Earth orbit. An artist's conception of a laser powered rocket is shown in Fig. 1.

Laser propulsion combines, in principle, the high specific impulse of nuclear or electric propulsion with the high thrust/weight ratio, and safety, of chemical rockets. Because the radiation absorbing propellant may be a high-temperature plasma, the specific impulse can be made very large. Because the energy source is on the ground, large payload/vehicle weight ratios are possible. These two fundamental advantages may only be exploited, of course, if two objectives are achieved. First, transmission of a well-collimated high-power laser beam must be accomplished; second, large lasers and power generation facilities must become both technically and economically feasible. A parametric analysis and optimization of possible missions along with estimates of cost per pound of payload have recently been made by Rom and Putre.[3]

In Ref. 4, a preliminary series of theoretical calculations and experiments were performed in order to determine the efficiency of converting laser power into thrust. Two methods for obtaining thrust by absorbing laser radiation were discussed. The first involved simply the rapid evaporation of a solid which absorbs the radiation to produce a jet of hot vapor. If, in addition, the vapor absorbs a fraction of the incident laser energy, it may be possible to obtain stagnation temperatures of 5000–12,000 K. By expanding this hot gas to convert all of the thermal energy into exhaust velocity, a specific impulse of 1000 sec seems feasible. If the vapor becomes fully ionized, the model of Basov et al.[5] predicts that a steady-state thrust can be achieved with a constant power laser when the plasma absorption length is of the order of

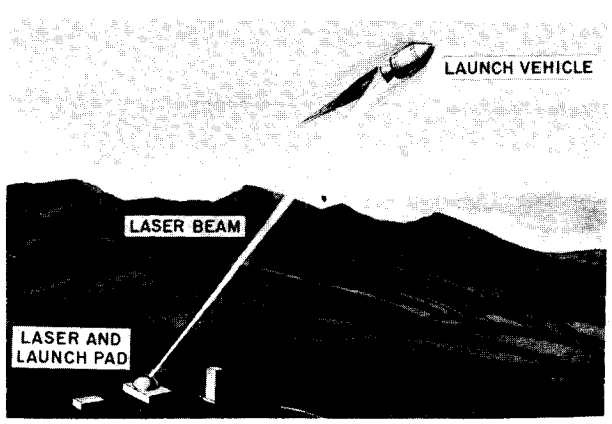

Fig. 1 Artist's conception of a laser-powered rocket.

Presented as Paper 73-624 at the AIAA 6th Fluid and Plasma Dynamics Conference, Palm Springs, Calif., July 16–18, 1973; submitted July 25, 1973; revision received April 10, 1974. This work was supported by the Advanced Research Projects Agency under Contract DAHC60-72-C-0131. The authors would like to thank A. R. Kantrowitz and P. K. Chapman for their suggestions and encouragement.

Index categories: Radiatively Coupled Flows and Heat Transfer; Lasers.

* Principal Research Scientist; presently Principal Scientist, Physical Sciences Inc., Wakefield, Mass. Member AIAA.

† Principal Research Scientist; presently Senior Scientist, Science Applications, Inc., Bedford, Mass.

‡ Senior Scientist; presently Principal Scientist, Physical Sciences Inc., Wakefield, Mass.

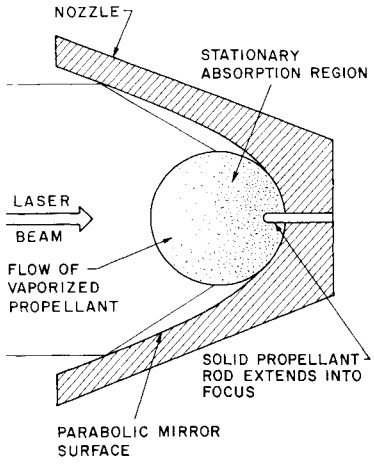

Fig. 2 Schematic of parabolic nozzle used in steady-state simulation experiments.

the beam diameter. In an atmosphere, however, the physics of the early time interaction between a high-power laser beam and a surface is strongly influenced by the presence of air above the surface. Before a steady-state jet of absorbing vapor can be obtained, the air above the surface may break down, and a radiation-driven (often called laser-supported) detonation wave may be initiated.[4,6] Once the wave forms, all of the laser radiation is absorbed in the shocked air behind the detonation, and the surface ablation stops. However, since this air is shocked to a high pressure, it may be possible to propel the vehicle by repetitively pulsing the laser and utilizing the strong detonation waves initiated with each pulse to provide thrust. This is the second method of using the absorption of laser radiation to power a rocket. By using the nozzle as a mirror, say in the form of a parabola, we can focus the transmitted laser power. Air breakdown then occurs in the focal region of the parabola. Thrust is obtained with no propellant other than the air which is present. If a means of replacing the air ionized during the breakdown process is provided between laser pulses, the thruster operates as a laser powered pulsejet. Preliminary experiments with this device were also discussed in Ref. 4.

In this paper, our progress toward a further understanding of the physics of the propulsion process is presented. Pulsed and steady-state experiments were performed utilizing a megawatt peak power, pulsed 10.6μ CO_2 laser. Steady-state simulation is obtained by making the size of the rocket nozzle such that the typical exhaust flow time is much less than the laser pulse time. The objective of the experiments was to measure the ratio of the thrust obtained to laser power (defined as the coupling coefficient) and the specific impulse, and determine the power conversion efficiency of both the solid propellant steady-state thrusting devices and the laser powered pulsejet. In Sec. II our steady-state experiments with both a simple ablation rocket and a more sophisticated device, which utilizes the parabolic nozzle to focus the transmitted laser power onto a solid propellant, are described. The data obtained with the laser powered pulsejet are presented in Sec. III. Section IV concludes with a discussion of future directions toward maximizing the efficiency of converting laser power to thrust.

II. Steady-State Propulsion Experiments

A steady-state laser propulsion system is a system whose thrust remains constant in time while the laser beam continuously provides the energy source for converting propellant potential energy to exhaust kinetic energy. The simplest propulsion system which accomplishes this consists of a solid propellant whose surface is continuously being vaporized by laser irradiation. The temperature of the vapor is dictated by the phase change of the propellant, and for most materials this temperature is approximately 1000–5000 K. At these temperatures the vapor is usually transparent to the incoming flux so that laser radiation continuously reaches the surface. It will be seen that this type of propulsion system offers a very high thrust per unit laser power. However, the exhaust velocity is limited since the maximum exhaust gas temperature is the temperature at which the propellant vaporizes. If the laser intensity is increased, the amount of ablated mass increases without increasing the exhaust velocity. Therefore, the rocket has a limited specific impulse, usually $\sim$100–200 sec. To increase the specific impulse and still preserve the steady-state nature of the flow, it is necessary to volumetrically add significant energy directly to the vapor. One possible way of doing this is shown schematically in Fig. 2.

The rocket nozzle in Fig. 2 utilizes a parabolic reflector which is both a mirror for the laser radiation and a nozzle for the exhaust gases. The parabolic reflector takes the incoming laser beam, whose flux magnitude will be below the maximum flux that can be propagated through the atmosphere, and focuses it upon a rod of solid propellant located at the focus. The vaporizing propellant thus passes through a region of high laser intensity ($\sim 10^7$–10^9 w/cm^2) and is heated to high temperatures. The high-temperature gas then expands converting its thermal energy to kinetic energy. This yields a higher specific impulse than the simple evaporation system. The drop in density and temperature in the expansion allows the exhaust to be transparent and the radiation to penetrate through to the subsonic region of the flowing vapor. If the high intensity region contains a plasma of unit optical depth ($KR \sim 1$), the flow will remain steady.

A. Experiment Configuration

Experiments were performed to examine the feasibility of the above concepts for steady-state laser powered propulsion systems. Since laser propulsion requires intensity and power levels higher than attainable with present day CW lasers, the experiments were performed with a 10.6 μ pulsed electron-beam sustainer type laser. This laser has a maximum 100 μsec pulse length and operates over a range of approximately 15–60 joules. It is possible to do steady-state experiments using a pulsed laser if the scale of the rocket nozzle is sufficiently small that there can be many flow times per pulse. Experiments were done first with a simple evaporating solid propellant consisting of Lucite and then with the parabolic reflector containing propellant rods of various materials.

Before the experiments are described, it is necessary to define the relevant parameters which determine the performance of these laser powered thrusters. The first important parameter is the coupling coefficient, which is the ratio of thrust to laser power. Since a pulsed laser was utilized, an average coupling coefficient is defined as

$$C = \int_o^{\tau_p} T(t)\,dt \Big/ g \int_o^{\tau_p} P(t)\,dt = I/E \tag{1}$$

Similarly, an average specific impulse is defined as

$$I_{sp} = u_e/g = \int_o^{\tau_p} T(t)\,dt \Big/ \int_o^{\tau_p} \dot{m}(t)\,dt = I/Mg \tag{2}$$

The efficiency of converting laser power to power in the exhaust is defined as

$$\eta = (\dot{m}u_e^2/2P) \tag{3}$$

For a value averaged over the pulse time, η can be written in terms of the coupling coefficient (expressed in mixed units of dynes/w) and the specific impulse (in units of seconds) as[4]

$$\eta = (5 \times 10^{-5})CI_{sp} \tag{4}$$

A ballistic pendulum was used to determine the impulse delivered to the thruster, and the propellant mass loss was obtained by weighing the solid propellant before and after each laser pulse. A typical power vs time history of the CO_2 laser pulse is presented in Fig. 3. This history was obtained by splitting off a small area of the beam and passing it into a gold-doped germanium detector. The power rises to a peak of 10^6 w

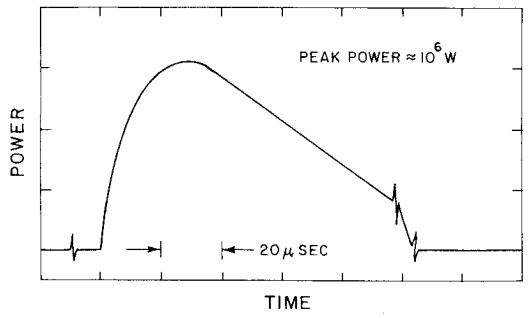

Fig. 3 Laser power vs time of 60 joule, 10.6 μ pulsed electron-beam laser.

after 25 μsec and decays gradually for the remainder of the 100 μsec pulse. The actual experimental arrangement is shown in Fig. 4. The major components are the laser, a vacuum box, and the pendulum. The vacuum box was made of clear Plexiglass with a salt window to admit the infrared radiation. The pressure was varied from 10^{-3}–1 atm, but all of the results presented, except for the first experiment with Lucite and no parabolic nozzle, were performed at the lowest pressure to eliminate the air effects on the thrust. The burn patterns shown in Fig. 4 were taken at the indicated stations to determine how the spatial distribution of intensity varies with distance, particularly up to the point where the beam enters the parabolic nozzle. When the nozzle was utilized, an auxiliary He-Ne laser was used (see Fig. 4) to illuminate a diffuse reflector on the back of the pendulum. The movement of the pendulum leaves a streak of light on the film of an open-shutter camera, corresponding to the greatest deflection. The deflection is then used to compute the impulse delivered.

B. Results

The first experiment was performed with a simple Lucite cylinder which had a hole in one end to form a nozzle. Since Lucite has a low vaporization temperature and its vapor does not ionize readily, it was anticipated that a steady-state jet of transparent vapor would result. The hole was 0.5 cm deep and 0.6 cm in diameter. The cylinder was placed in the ballistic pendulum arrangement and from the pendulum deflection a coupling coefficient of 92 dynes/w was calculated. By weighing

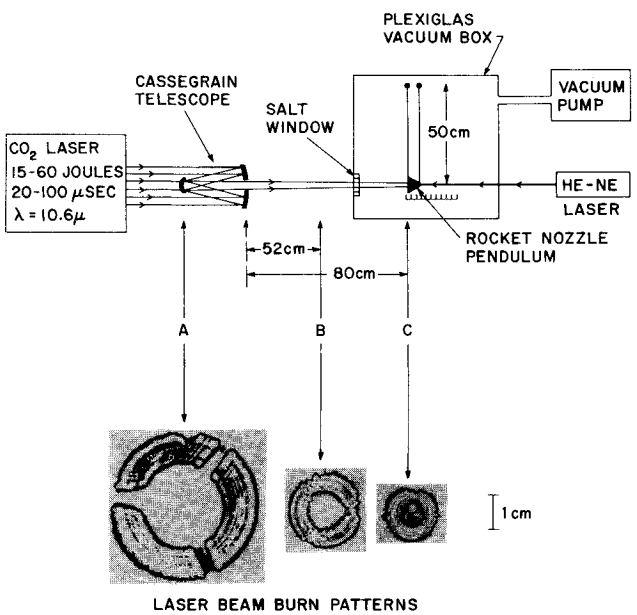

Fig. 4 Experimental arrangement for steady-state simulation experiment.

the cylinder before and after, and using Eq. (2), we obtained a specific impulse of 88 sec, and an exhaust velocity of approximately 9×10^4 cm/sec. Thus, the ratio of laser pulse time to flow time was approximately 18, sufficiently long to insure steady-state propulsion. The simple Lucite rocket achieved a large thrust to laser power ratio from a large mass flow of propellant. The power conversion efficiency, from Eq. (4), was approximately 40%.

The remaining experiments were performed with the parabolic reflecting nozzle since our objective was to obtain a high specific impulse. The nozzles used were made of copper, and the parabolic surface was gold coated. Both the exit plane diameter and the length of the nozzle were approximately 2.5 cm. The nozzle itself weighed 35 g, and solid propellant rods of various composition extended into the focus of the parabolic reflector. The rods were 0.075–0.15 cm in diameter, and the laser intensity upon the surface of the rods was calculated to be $1–5 \times 10^7$ w/cm^2. Propellant rods of Lucite, graphite and lithium fluoride were used in these experiments.

The results of the measurements of coupling coefficient and specific impulse are summarized in Fig. 5. Typical pendulum deflections were from 0.5 to 3 cm, and propellant mass losses ranged from 0.5 to 1 mg. The scatter in the data along with a 5% error in reading the deflections is incorporated into the shaded regions of the graph. Lines of constant power conversion efficiency are also drawn. It can be seen that the highest specific impulse was obtained with graphite and ranged from 100–500 sec. The coupling coefficient was between 2–3 dynes/w. These parameters yield [from Eq. (4)] a power conversion efficiency of 2–7%.

An unfortunate feature of graphite was that it would condense on the walls of the parabolic nozzle, and invariably one-third of the vaporized carbon provided thrust while two thirds condensed on the nozzle walls. Only the propellant mass which left the exit plane of the nozzle was considered when computing the specific impulse. Clearly, condensation on the mirror surface of the nozzle is detrimental for steady-state operation, and solid propellants whose vapor products remain gaseous upon expansion must be used. Lucite did not condense as much as graphite and only a small amount of condensate (compared to total mass evaporated) was found at the vertex of the parabola. The coupling coefficients for the Lucite experiments were significantly higher than for graphite, but the specific impulse did not exceed 200 sec. The propellant rod was often consumed, while the graphite propellant rod only suffered a layer of mass loss near the focus. The conversion efficiency with Lucite was approximately 10–20%. For comparison, the results obtained with the plastic Lucite cylinder, described above, are also presented in Fig. 5. The lower laser intensity resulted in a higher coupling coefficient with lower specific impulse. However, the power conversion efficiency was a factor of two higher. The experiments performed in the parabolic nozzle resulted in higher specific impulse and thus, there may have been heating of the vapor with the higher laser intensities. The lower efficiency is unexplained, but may be a result of

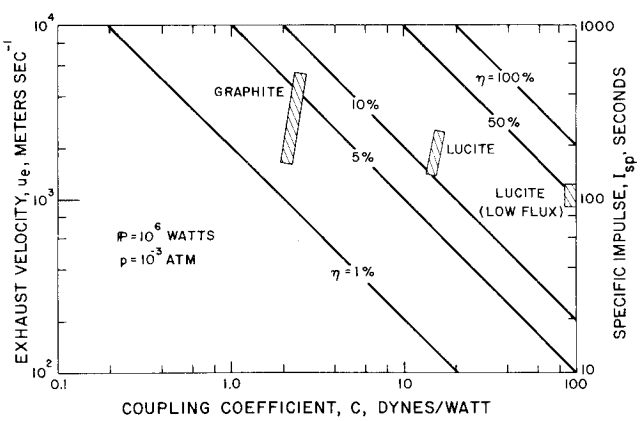

Fig. 5 Summary of coupling coefficient and specific impulse results.

increased losses when the propellant vapor is heated. No nozzleless experiments were performed under similar conditions with graphite; however, published results[7,8] for ruby laser irradiation of graphite in vacuum indicate similar values for coupling coefficient, but much higher particle velocities. However, pulse times were much shorter,[7,8] resulting in extremely high intensities, and no clear comparison can be made.

The values of specific impulse obtained in the above experiments are not as high as desirable for projected applications of laser propulsion.[1-4] It appears that with graphite and Lucite as propellants insufficient heating took place in the vapor and the results were more characteristic of steady-state jetting of an essentially transparent vapor. This was confirmed by a drum camera photograph of the vapor exhausted from a nozzle containing a graphite propellant rod. This photograph is presented in Fig. 6a. The lower left corner of the luminous region corresponds to the exit plane of the nozzle at close to time equal zero. The observed luminosity in Fig. 6a indicates a fairly uniform exhaust throughout the 100 μsec laser pulse. This is characteristic of steady-state vaporization of the propellant; however, the average exhaust velocity deduced from the measured specific impulse corresponds to a stagnation temperature only slightly higher than the vaporization temperature of graphite at several atmospheres pressure. Therefore, it appears that there was insufficient heating of the graphite vapor to obtain a specific impulse of 1000 sec or greater. In order to increase the vapor absorption, experiments were performed with lithium fluoride. Lithium fluoride is a low molecular weight solid which is stable in a laboratory atmosphere. Lithium is easily ionized and will absorb strongly via inverse bremsstrahlung. Lithium fluoride propellant rods were inserted into the parabolic nozzle; however, results for coupling coefficient and specific impulse were not significantly measurable. The results were not plotted in Fig. 5, and drum camera photographs indicate that the poor performance was a result of the initiation of strong laser-supported absorption waves in the vapor. A typical photograph is presented in Fig. 6b. Because of strong vapor absorption, immediately after the propellant rod begins to evaporate, a laser-supported detonation wave[4,6] was initiated. The vaporization stops, and the wave can be seen to propagate up the laser beam. The resulting nozzle flow was unsteady, and over the 100 μsec pulse time, negligible average thrust was recorded. In some cases, after the first detonation wave was initiated, it propagated up the laser beam until the vapor became transparent. Subsequently, more propellant evaporated and a second wave was initiated which again propagated up the beam until it expanded. The process repeated leading to pulsating flow and a low average specific impulse.

The reason for the observations described above along with a proper choice of operating conditions for steady-state propulsion, can be deduced by examining the absorption characteristics of the propellant vapor. A typical calculated coefficient for the absorption of 10.6 μ laser radiation by inverse bremsstrahlung is

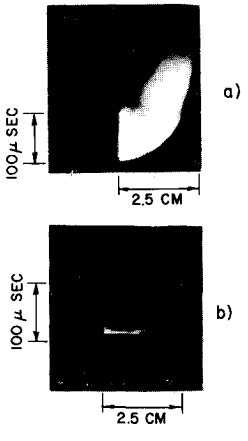

Fig. 6 Rotating drum camera photographs of exhaust from parabolic nozzle. a) Graphite, $E = 42$ joules. b) Lithium fluoride, $E = 31$ joules.

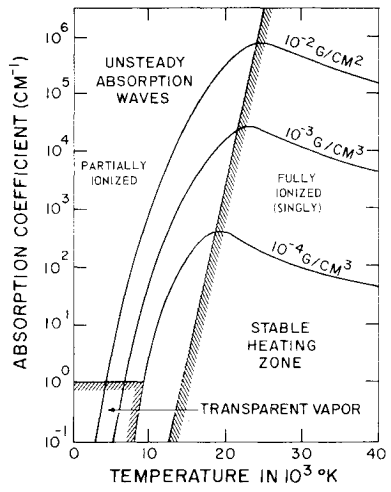

Fig. 7 Inverse bremsstrahlung absorption coefficient of carbon vs temperature for 10.6 μ radiation.

presented in Fig. 7. This particular calculation was made utilizing relations for neutral-electron and ion-electron inverse bremsstrahlung presented in Ref. 9. Figure 7 presents the absorption coefficient of carbon vapor as a function of temperature for three values of vapor density. The rapid rise in the absorption coefficient with increasing temperature at constant density occurs when the vapor is only partially ionized. Once the vapor becomes fully ionized the absorption coefficient $\sim T^{-3/2}$. In the partially ionized region the absorption is both neutral-electron and ion-electron inverse bremsstrahlung while in the fully ionized region absorption is solely via ion-electron interactions. Initially, when the propellant vaporizes, the vapor is transparent; the absorption coefficient at the initial vaporization temperature and corresponding density is in the partially ionized region labeled "transparent vapor" in Fig. 7. The value of the heating rate depends upon the magnitude of the absorption coefficient and will either be too small to result in significant heating (e.g., graphite and Lucite) or be sufficiently large to start a rapid rise up the absorption curve. The vapor rapidly becomes opaque and absorption waves are generated leading to unsteady flow (e.g., lithium fluoride). Stable heating will occur when the vapor is fully ionized so when the gas is heated further, it becomes more transparent. The heating zone will remain stationary a short distance above the surface in the expanding flowfield.

We can conclude from the above discussion that steady-state propulsion will be best achieved with a propellant whose vapor absorption coefficient (either from inverse bremsstrahlung or other absorption mechanisms) is large and decreases with increasing temperature. For a propellant that absorbs via inverse bremsstrahlung, an ideal propellant may consist of a low molecular weight substance that contains a small fraction of easily ionized seed (e.g., H_2 or He plus Li or Cs). The seed becomes fully ionized and transfers energy to the low molecular weight species, accelerating it to a high velocity.

III. Pulsed Propulsion Experiments

In Sec. II, efforts to obtain a steady-state thrust and high specific impulse with a laser were described. It was shown that in order to obtain steady thrust with high specific impulse and high efficiency, it is necessary to design a system in which the high-temperature plasma remains stable. Any oscillatory behavior in the absorption zone will lead to inefficiency and a pulsating phenomena. If an unstable absorption zone leads to a low efficiency rocket, it may be possible to obtain significant thrust at a high specific impulse by pulsing the laser.

The way to obtain large thrust and high specific impulse with a pulsed laser that is discussed here is an outgrowth of various

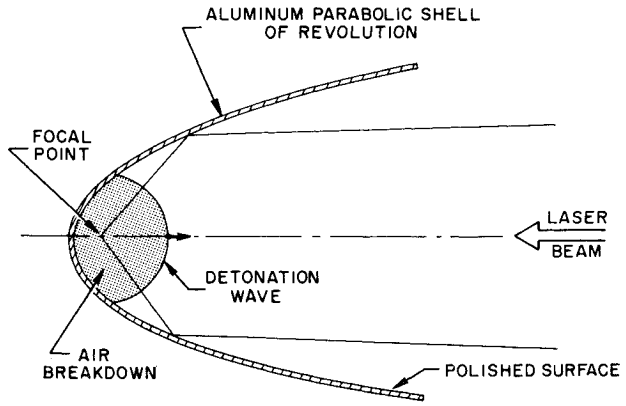

Fig. 8 Laser-powered pulsejet.

experimental and theoretical programs in laser effects.[6,10-13] It was found by researchers that when a high power laser is focused to a large flux on a surface in an atmosphere, a highly absorbing plasma forms and a relatively high coupling coefficient is obtained with very little mass loss. It has been concluded that the high radiation flux leads to a breakdown above the surface of either the small amount of vaporized material or contaminated air above the surface, and a laser-supported detonation wave, which propagates up the laser beam, is initiated. The high pressure behind this wave yields a significant force on the surface and thus thrust may be obtained with only air as the propellant. Provided the pulse is sufficiently short that the high pressure region remains in the vicinity of the surface, this method may be an efficient propulsion mechanism. An additional effect is that after the laser beam is turned off, since the force is a result of shocking the air above the surface, there exists a time over which the high pressure gas relaxes to one atmosphere. Thus, there is thrust after the laser pulse terminates. A combination of this result plus the use of air as a propellant leads one to explore the possibility of a pulsejet for a propulsion system in the atmosphere. In space, obtaining thrust by initiating a succession of breakdowns in a nozzle with a pulsing laser requires that the fuel be supplied from an on-board system.

A. Laser Powered Pulsejet Concept

A schematic of the laser powered pulsejet concept is shown in Fig. 8. By containing the shocked air within a nozzle, a greater amount of the over-all shock kinetic energy is directed into force, and the air specific impulse is increased. When the nozzle is parabolic, the laser energy impinging upon the polished inner surface is focused to a high flux. The subsequent air breakdown initiates the detonation wave and this wave propagates toward the exit of the nozzle, converting all of the high pressure gas behind it into a force on the nozzle wall. Thrust is obtained for the time it takes the wave to propagate down the wall to the exit plane of the nozzle. Since this time can be much longer than the laser pulse time, we must redefine the average power conversion efficiency. In Eq. (2) the integrals are now over the thrusting time instead of the laser pulse time, and in Eq. (1) the integral in the numerator is over the thrusting time while the integral of the laser power remains over the pulse time; Eq. (4) remains unchanged. The coupling coefficient in dyne-sec/joule is now in terms of the over-all impulse delivered to the nozzle. In Ref. 4 the maximum measured value of the coupling coefficient was 40 dyne-sec/joule for a 60 joule, 25 μsec laser pulse. This value decreased to approximately 15 dyne-sec/joule when the energy was increased to 300 joule with a 25 μsec pulse. It is believed that the decrease in the coupling with increase in laser energy was because the laser beam area at the nozzle exit plane was much smaller than the exit plane area. The average laser flux at the nozzle exit was 5×10^6–10^7 w/cm^2. This flux was sufficient to sustain the laser-supported detonation wave initiated by the breakdown; the wave raced out of the nozzle, decreasing the coupling coefficient.

The present experiments were performed to determine the dependence of the coupling coefficient upon the beam area at the entrance to the nozzle, laser energy, and pulse time. It was desirable to obtain as much information as possible from a single pulse experiment in order to assess how efficient a propulsion device a multiple-pulsed pulsejet becomes. The 60 joule, 10.6 μ, 100 μsec pulse electron-beam laser was also used for this experiment. However, these experiments were performed in laboratory air, and the focal length of the telescope was made as large as possible to insure a close to parallel beam. The principal diagnostics included a ballistic pendulum, in order to determine the over-all impulse delivered, and a rotating drum camera, in order to observe the plasma formation in the nozzle. In addition, pressure transducer stations were placed at various points along the wall of the nozzle in order to monitor the pressure vs time history throughout the thrusting pulse.

B. Experimental Procedure

The beam directly from the optical telescope of the laser was passed into an aluminum parabolic nozzle similar to that in Fig. 8. The nozzle was 10.5 cm long and had an exit plane diameter $\approx$7 cm. It was initially desired to utilize the beam area equal to the exit area of the nozzle; however, when a beam of this size was passed into the nozzle, no breakdown was observed. Since the beam area under these conditions is approximately 35 cm^2, the peak flux is only of the order of tens of kilowatts per square centimeter at the exit plane. The optical quality of the parabola is apparently not sufficient to ensure a high enough flux in the focal region to cause a breakdown. Polished aluminum has a reflectivity > 0.9 at 10.6 μ; however, it was found that any oxide coating on the inner linings of the parabola would yield sufficient absorption of the beam to further reduce the peak flux at the focus. Occasionally, a breakdown was obtained and thrust was measured after the inside of the parabola was cleaned with an abrasive material. The beam area at the exit plane was then reduced until a consistent breakdown and measurable thrust was obtained. This was then considered to be the largest beam area that would yield significant data. With this area as a reference, the beam area was reduced and dependence of the coupling coefficient upon beam area was recorded. Four beam areas were experimented with, the areas ranging from 5 cm^2 down to 1.5 cm^2. The lowest average flux at the exit plane of the nozzle was $\sim 10^5$ w/cm^2.

C. Coupling Coefficient and Surface Pressure Results

A plot of the coupling coefficient vs energy is presented in Fig. 9. The laser was operated in the energy range from 10 to 60 joules and the pulse time was varied between 25–100 μsec. The open points shown in Fig. 9 denote the coupling coefficient obtained when the peak power of the laser was kept constant and the energy was varied by changing the pulse time: the solid points are those results obtained when the energy was reduced by lowering the peak power at a fixed pulse time of 100 μsec. The results are shown for the different beam areas ranging from 5 cm^2 down to 1.5 cm^2. It can be seen that when the peak power was constant, the coupling coefficient with the smallest beam areas was approximately constant with increase in energy, while with the largest beam area there was a significant scatter in the coupling coefficient data as the energy was increased from 40 to 60 joules. Since occasionally a failure to break down the air was observed with the larger beam sizes, the scatter in the coupling coefficient data for the 5 cm^2 beam can probably be attributed to the poor optical quality of the parabola along with oxide formation on the surface. It is felt that only the smallest beam area results represent meaningful data. When the pulse time was maintained at 100 μsec and the peak power varied (solid points), the coupling increased by approximately a factor of 3 when the energy was doubled. Since breakdown and plasma heating is flux dependent, this result is not surprising. However, the rate of rise of the coefficient is not easily explained. Coupling coefficients of

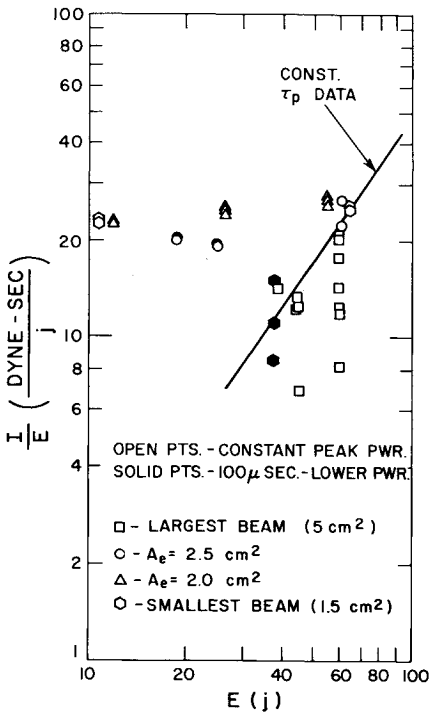

Fig. 9 Coupling coefficient results for pulsejet experiment.

25–40 dyne-sec/joule have been reported previously,[4,14] but only with a nozzle arrangement containing the plasma. Nozzleless results[10–13] obtained off flat surfaces have not exceeded 10 dyne-sec/joule.

Celesco LD-25 pressure transducers with a 1 μsec response time were placed into holes drilled in the wall of the nozzle at several stations. The transducer surfaces were located flush with the inside wall of the nozzle and were acoustically insulated from the wall. Typical results for the pressure profiles are presented in Fig. 10. The location of each station is indicated by its distance x measured along the nozzle axis from the nozzle nose toward the exit plane. The results are for a 60 joule, 100 μsec laser pulse. Time is 50 μsec per division and for each photograph the lower curve denotes the pressure transducer trace while the upper curve denotes what was seen by a photodiode detector mounted facing into the nozzle exhaust at an angle to the axis. Thus, a rise in the photodiode trace indicates the presence of a luminous plasma. The blip at the left of the pressure trace denotes the turn-on of the laser sustainer and electron-beam voltages. The laser pulse begins approximately 20 μsec after this time and at this point a luminous plasma can be seen and is detected by the photodiode. Shortly thereafter, the pressure wave generated by the breakdown passes the first station. This is followed by a region of gas absorption and a slight rarefaction before the pressure at Station 1 relaxes to ambient. Station 2 indicates a similar profile only beginning at a time approximately 100 μsec after the laser pulse begins. In the trace labeled Station 3, the turn-off of the laser pulse can be seen and is indicated by the two blips approximately 120 μsec after the electron-beam and sustainer voltages were turned on. It should be pointed out that between Stations 1–4, the scale on the vertical axis is positive down and was changed in order to increase the resolution; therefore, one should not interpret the increasing peaks as an actual increase in the peak pressure amplitude. The actual peak pressure values are indicated to the right of each photograph. After the laser pulse has terminated, the gas then relaxes and the trace at Station 4 (the exit plane of the nozzle) resembles more closely that of a classical shock wave followed by an expansion fan. This is the profile that would be expected as the shocked gas emerges from the nozzle. The end of the laser pulse is also coincident with a decrease in the luminosity of the plasma, as can be seen from the photodiode traces at Stations 1–4.

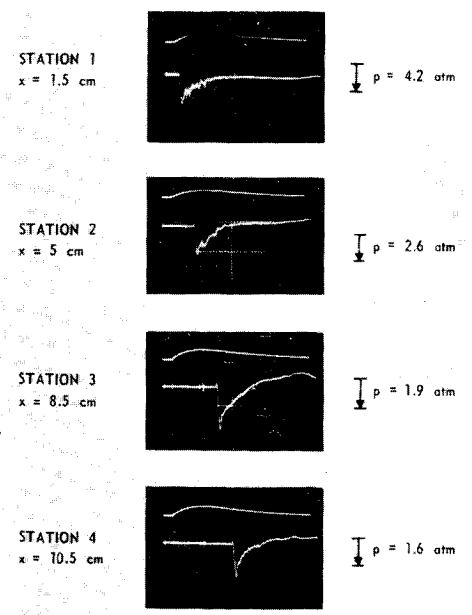

Fig. 10 Pressure transducer traces. $E = 60$ joules, $\tau_p = 100$ μsec, 50 μsec/div. in time.

The most significant result to come from the pressure traces is the observed small pressure rise across the shock wave as it propagates down the nozzle. Nowhere does the peak pressure rise above 4.2 atm. This can be seen more dramatically in Fig. 11 where the pressure jump across the shock is plotted as a function of position x as the wave propagates toward the exit plane. The low peak pressure implies that the initial shock produced by the breakdown was fairly weak by the time it reached the first station. Only a small fraction of the total laser energy has apparently gone into the initial breakdown volume and the remainder of the laser pulse is volumetrically absorbed in the gas behind the shock as it propagates down the nozzle. It can also be seen from Fig. 11 that when the power was kept constant and the pulse time varied, the peak pressure was virtually unchanged. This supports the hypothesis that increasing the pulse time only increased the amount of energy volumetrically absorbed in the gas behind the shock produced by the breakdown. Also, as the peak power was reduced to two-thirds its value, the peak pressure decreased. Thus, the peak pressure in the

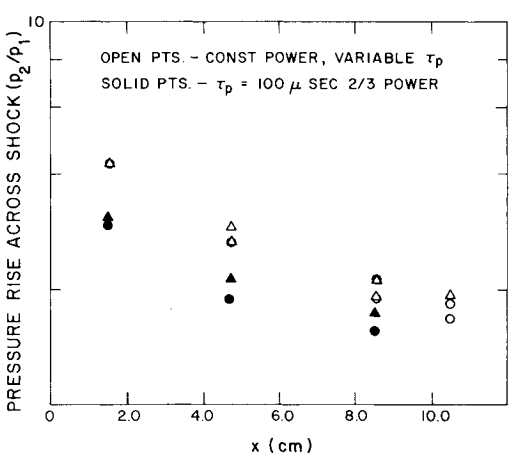

Fig. 11 Peak pressure behind shock wave vs axial position in nozzle.

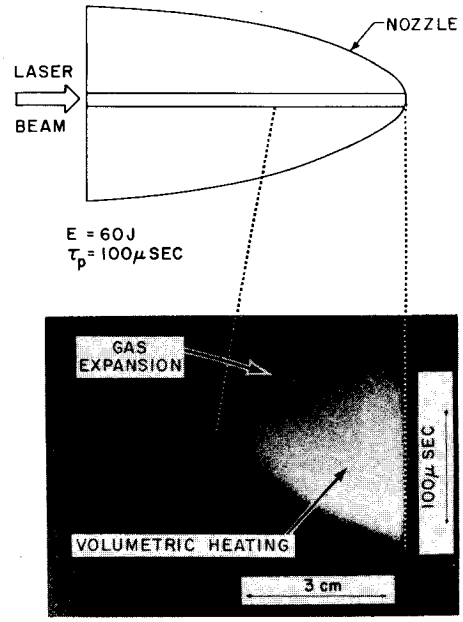

Fig. 12 Schematic of arrangement for drum camera photographs and actual observed plasma formation.

wave is essentially power dependent. This is consistent with a breakdown formulation for the energy source. A reduction of the power by two-thirds yields approximately an equivalent reduction in the peak pressure at the stations along the wall.

D. Plasma Formation

A rotating drum camera was used to observe the formation of the plasma in the nozzle. The slit was cut along the axis of the nozzle as is shown in Fig. 12. From the observations, the average velocity of the luminous front along with the volume of air that was heated can be deduced.

The photograph in Fig. 12 shows the time evolution of the plasma produced in the nozzle when the laser energy was 60 joules and the pulse time was approximately 100 μsec. Time $t = 0$ at the focus of the parabola is the lower right-hand corner of the luminous region. The time and position axes are noted, and for the 100 μsec laser pulse the plasma has propagated 3 cm toward the exit plane. The average velocity of the leading edge of the luminous region is approximately 5×10^4 cm/sec, and the average laser flux approximately 3×10^5 w/cm^2. Since the beam area at the exit plane is only 2 cm^2, the flux is still constant throughout the observed region and thus, the position vs time trajectory of the leading edge is fairly straight. From the photograph it appears that after the laser pulse has ended, the expansion of the gas yields a cooling of the plasma from the plasma leading edge toward the nozzle nose. From Fig. 11 the pressure ratio across the shock is ≈ 3, and using shock tables this corresponds to a shock Mach number of approximately 1.6. This is consistent with the observed velocity of the leading edge of the plasma which corresponds to a Mach number ≈ 1.5. The shock wave is weak and the laser energy is dumped volumetrically into the gas behind the wave. The flux is not high enough to sustain a classical laser-supported detonation wave, where the laser energy is absorbed in a thin region directly behind the shock. It can be seen from Fig. 12 that the luminosity behind the leading edge of the plasma is fairly constant and thus the plasma is probably optically thin to the laser radiation. The shocked gas is absorbing radiation almost uniformly.

E. Power Conversion Efficiency

From Eq. (4) the power conversion efficiency is proportional to the product of the coupling coefficient and specific impulse. The specific impulse depends upon the mass of air that is utilized to obtain thrust. More specifically, for the present experiments, this mass is the mass of air that has exited the nozzle as a result of the thrusting process. For the case of the laser energy equal to 60 joules and a pulse time of 100 μsec, this mass can be calculated by utilizing the pressure trace at Station 4 in Fig. 10. At every time when the overpressure is greater than unity, the particle velocity is positive. In the exit plane every particle with a positive velocity will exit the nozzle. The density profile and particle velocity profile which corresponds to the observed pressure trace can be estimated by using the normal shock equations. From Fig. 10, the pressure ratio across the shock when it crosses the exit plane $p_2/p_1 \approx 1.6$ to 2.0, where p_2 is the pressure immediately behind the shock and p_1 denotes the ambient pressure. From shock tables the shock Mach number ≈ 1.37 and the density and particle velocity immediately behind the shock wave become $\rho_2/\rho_1 \approx 1.6$ and $u \approx 1.9 \times 10^4$ cm/sec. Now, the mass of air that exits the nozzle can be written

$$M_a = \int_o^{\tau_e} \rho_e u_e A_e dt \tag{5}$$

ρ_e and u_e are functions of time and are determined from the shock profile. τ_e denotes the time period during which mass is being expelled from the nozzle. From Fig. 10, $\tau_e \approx 75$ μsec. Assuming a linear profile for the properties behind the shock, we can write

$$\begin{aligned} \rho_e &= \rho_2\{1-([1-(\rho_1/\rho_2)]/\tau_e)t\} \\ u_e &= u[1-(t/\tau_e)] \end{aligned} \tag{6}$$

Substituting Eq. (6) into (5) and using $\rho_2/\rho_1 = 1.603$, $\rho_1 = 1.25 \times 10^{-3}$ g/cm^3, $u = 1.9 \times 10^4$ cm/sec, $\tau_e \approx 75$ μsec, we obtain $M_a \approx 47$ mg of air. Substituting a coupling coefficient of 25 dyne-sec/joule, $I = 1500$ dyne-sec and $M_a = 47$ mg into Eqs. (2) and (4) we obtain a power conversion efficiency of approximately 4%. This is a much lower efficiency than we had hoped to obtain with this device. However, the pressure and plasma observations indicate that the low efficiency is a result of the long laser pulse. By using a long pulse laser, more laser energy was converted into volumetric heating of a large volume of gas instead of creating a high pressure behind a laser-supported detonation wave. It was also found, by measuring the wall temperatures, that much of the hot plasma conducted its heat to the nozzle wall. As much as one-third of the laser energy may have ended up in the nozzle wall.

IV. Summary and Conclusions

Experiments were performed to simulate the physics of propulsion by absorption of radiation from a remotely stationed high-power CW or pulsed laser. The steady-state experiments were done with solid propellants, and the results indicate that a high ratio of thrust to laser power can be obtained by simply using the laser to vaporize a solid surface. However, in order to obtain a high specific impulse it is necessary to add energy to the vapor in a stable manner. The best way to do this seems to be to utilize a gas propellant which has been seeded to provide some external control over the absorption characteristics. A mixture of low molecular weight propellant and a small percentage of an easily ionizable alkali metal as a seed may provide the characteristics necessary to obtain a stable heating zone in a throatless nozzle. Recently, Buonadonna et al.[15] have described a laser heated wind tunnel where the gas is heated upstream of the throat of a standard nozzle by passing the beam through a window. For propulsion this would eliminate the need for a throatless nozzle. However, it would require a window material that will tolerate transmission of significant laser intensities along with high pressures and temperatures for long periods of time.

The pulsed laser experiments were performed with the laser-powered pulsejet configuration. Thrust was obtained by initiating an air breakdown in the nozzle, and low power conversion efficiency was characteristic of a long, low-power laser pulse. A high ratio of thrust to laser power was obtained when compared with results obtained for breakdown above surfaces. By shorting

the pulse, an increase in the efficiency of mass utilization may be expected. Thus, future experiments should be done with higher power, shorter pulse lasers. The advantage of a short-pulse system is that the thrusting time will be much greater than the pulse time, and quasi-steady thrust may be obtainable by a series of short laser pulses such that each succeeding thrusting pulse begins before the previous one ends. It is necessary, however, to design an efficient propellant feed system to complete this system.

References

[1] Kantrowitz, A. R., "The Relevance of Space," *Aeronautics & Astronautics*, Vol. 9, No. 3, March 1971, p. 35.

[2] Kantrowitz, A. R., "Propulsion to Orbit by Ground-Based Lasers," *Aeronautics & Astronautics*, Vol. 10. No. 5, May 1972, p. 74.

[3] Rom, F. E. and Putre, H. A., "Laser Propulsion," TM-X-2510, April 1972, NASA.

[4] Pirri, A. N. and Weiss, R. F., "Laser Propulsion," AIAA Paper 72-719, Boston, Mass., 1972.

[5] Basov, N. G., Gribkov, V. A., Krokhin, O. N., and Sklizkov, G. V., "High Temperature Effects of Intense Laser Emission Focused on a Solid Target," *Soviet Physics—JETP*, Vol. 27, No. 4, Oct. 1968, p. 575.

[6] Pirri, A. N., Schlier, R., and Northam, D., "Momentum Transfer and Plasma Formation Above a Surface with a High-Power CO_2 Laser," *Applied Physics Letters*, Vol. 21, No. 3, Aug. 1972, pp. 79–81.

[7] Gregg, D. W. and Thomas, S. J., "Momentum Transfer Produced by Focused Laser Giant Pulses," *Journal of Applied Physics*, Vol. 37, No. 7, June 1966, pp. 2787–2789.

[8] Gregg, D. W. and Thomas, S. J., "Kinetic Energies of Ions Produced by Laser Giant Pulses," *Journal of Applied Physics*, Vol. 37, No. 12, Nov. 1966, pp. 4313–4316.

[9] Zel'dovich, Y. B. and Raizer, Y. P., *Physics of Shock Waves and High-Temperature Hydrodynamic Phenomena*, Academic Press, New York, 1966, pp. 258–283.

[10] Lowder, J. E., Lencioni, D. E., Hilton, T. W., and Hull, R. J., "High-Energy Pulsed CO_2 Laser-Target Interaction in Air," *Journal of Applied Physics*, Vol. 44, No. 6, June 1973, p. 2759.

[11] Pirri, A. N., "Theory for Momentum Transfer to a Surface with a High-Power Laser," *The Physics of Fluids*, Vol. 16, No. 9, Sept. 1973, p. 1435.

[12] Hall, R. B., Maher, W. E., and Wei, P. S. P., "An Investigation of Laser-Supported Detonation Waves," AFWL-TR-73-28, June 1973, Air Force Weapons Lab., N.Mex.

[13] Hettche, L. R., Schriempf, J. T., and Stegman, R. L., "Impulse Reaction Resulting from the In-Air Irradiation of Aluminum by a Pulsed CO_2 Laser," *Journal of Applied Physics*, Vol. 44, No. 9, Sept. 1973, p. 4079.

[14] Barchukov, A. I., Bunkin, F. V., Konov, V. I., and Prokhorov, A. M., "Low-Threshold Breakdown of Air near a Target by CO_2 Radiation, and the Associated Large Recoil Momentum," *JETP Letters*, Vol. 17, No. 8, April 20, 1973, p. 294.

[15] Buonadonna, V. R., Knight, C. J., and Hertzberg, A., "The Laser Heated Wind Tunnel," *AIAA Journal*, Vol. 11, No. 11, Nov. 1973, pp. 1457–1458.

SEPTEMBER 1974 AIAA JOURNAL VOL. 12, NO. 9

Heat Pipe Model Accounting for Variable Evaporator and Condenser Lengths

C. L. WILLIAMS*
Westinghouse Electric Corporation, Pittsburgh, Pa.

AND

G. T. COLWELL†
Georgia Institute of Technology, Atlanta, Ga.

A correlation model is established for the steady-state performance of a horizontal heat pipe operating below the capillary limited heat rate and with internally self adjusting evaporator and condenser lengths. The length along which condensation occurs is found to depend on the axial vapor Reynolds number. The partially saturated evaporator length, and the corresponding length along which evaporation occurs is found to depend on the detail wick geometry and the evaporator meniscus radius. These dependencies are corroborated by experimental data from a cylindrical heat pipe with working fluids of water and methanol. The experimental wick consists of two layers of 100 mesh stainless steel screen separated by a thin liquid region. Comparison of correlation predictions to experimental results of this study and others show agreement to within 15%.

Nomenclature

A_w = wick total cross-sectional area, ft^2
f = function
h_{vl} = latent heat of vaporization, btu/lbm
K_{eff} = effective wick thermal conductivity for two layers of screen (btu/hr ft °R)
K_l = liquid thermal conductivity, (btu/hr ft °R)
K_s = wick solid thermal conductivity, (btu/hr ft °R)
K_w = effective wick thermal conductivity for one layer of screen, (btu/hr ft^2 °R)
K = wick friction factor (inverse permeability), 1/ft^2
l_{eff} = liquid effective frictional length, ft
l = design length, ft
L = active length, ft
$\dot{m}$ = mass flow rate, lbm/hr
n = number of layers of screen
P = pressure, lbf/ft^2 absolute
$\dot{Q}_e$ = evaporator heat-transfer rate, btu/hr
r_c = wick pore radius, ft
r_m = evaporator meniscus radius, ft
r_v = vapor space radius from heat pipe axis, ft
r_w = outer radius of wick, ft
r_{ws} = wick-solid radius (one-half wire diameter for mesh screen), ft
Re = Reynolds number
$\bar{T}_{ew}$ = evaporator average temperature at outer wick surface, °R

Received September 10, 1973; revision received February 26, 1974. This work was performed on a Ph.D. thesis during graduate study at Georgia Institute of Technology.

Index categories: Heat Conduction; Thermal Modeling and Experimental Thermal Simulation.

* Senior Engineer, Bettis Atomic Power Laboratory.

† Associate Professor, School of Mechanical Engineering.